SF2A 2022
J. Richard, A. Siebert, E. Lagadec, N. Lagarde, O. Venot, J. Malzac, J.-B. Marquette, M. N'Diaye, D. Briot (eds)

SPATIAL DISCONNECTION BETWEEN STELLAR AND DUST EMISSIONS: THE TEST OF THE ANTENNAE GALAXIES (ARP 244)

L.-M. Seillé[1], V. Buat[1,2], W. Haddad[1], A. Boselli[1], M. Boquien[3], L. Ciesla[1], Y. Roehlly[1] and D. Burgarella[1]

Abstract.
Star formation rate (SFR) and stellar mass estimations of galaxies computed using integrated data can be impacted by strong local variations of stellar and dust distributions. Numerous distant dust-obscured galaxies exhibiting disturbed morphologies have been observed and we propose to use the Antennae Galaxies as a resolved local proxy for z $\sim$ 2 galaxies. We combine GALEX, Pan-STARRS, VISTA, *Spitzer* and *Herschel* images of the Antennae Galaxies to study the variations of the broadband spectral energy distributions (SEDs) of 58 $\sim$ 1 kpc size regions in this nearby prototypical major merger. We compare the estimates of the SFR and stellar mass of the galaxies as a whole to the SFR and stellar mass estimates of the 58 regions altogether. We discuss the difference found between the different estimations in relation to the very complex dust attenuation process going on in the Overlap regions.

Keywords: galaxies, ISM, SED fitting, Arp 244

1 Introduction

Dust can drastically change the shape of the ultraviolet (UV) to near-infrared (IR) SED as it absorbs photons and thermally re-emits the absorbed energy in the infrared. That is why SED modelling codes apply the energy balance principle: the energy radiated by dust corresponds to the energy of the absorbed stellar light.

To take this effect into account, people introduced attenuation recipes to redden the stellar continuum, the most common ones being the Calzetti attenuation curve (Calzetti et al. 2000) and the recipe of Charlot & Fall (Charlot & Fall 2000) with a power-law dependence of the effective attenuation with wavelength. However, both observational and theoretical studies lead to the conclusion that a single attenuation curve does not account for all star-forming galaxies and that more flexible curves are required.

In 2018, Elbaz et al. (2018) used ALMA to observe high-redshift massive dusty galaxies with a very compact dust emission and a clumpy rest-frame UV emission, located far away from the dust emission. These detections question the validity of a local energy balance which is still expected to be valid at a global scale. This issue is critical as the way stellar and dust emissions are linked is expected to have an impact on the physical parameters derived from the spectral energy distribution modelling of the global emission. In this work, we focus on the progenitors of Antennae Galaxies also known as NGC 4038/NGC 4039 or Arp 244 which are a pair of interacting galaxies exhibiting very different UV and IR spatial distribution like the dusty high-redshift galaxies observed with ALMA. Their proximity, allows for a multi-wavelength UV to far-IR study at a kpc scale.

We use the Antennae Galaxies as a proxy to test the validity of SED modelling techniques based on energy conservation in high redshift dusty galaxies with complex geometry. We also investigate the similarity of global and local measurements of physical quantities and infer what information can be reliably retrieved from the analysis of the full SED.

[1] Aix-Marseille Univ, CNRS, CNES, LAM, Marseille, France
[2] Institut Universitaire de France (IUF)
[3] Centro de Astronomía (CITEVA), Universidad de Antofagasta, Avenida Angamos 601, Antofagasta, Chile

2 Photometry

We retrieved 15 images of the Antennae Galaxies from the UV to the far-IR. The images are degraded to the lowest resolution and pixel size of our dataset which corresponds to the 160 μm image. After that, we convolve all the other images to reach this resolution and reproject them. At the end of the process, all the images have the same size, orientation, pixel size and resolution. The images are then divided into square boxes sampling a physical area of 1.3 kpc^2 and we call each box a "region" (Fig. 1).

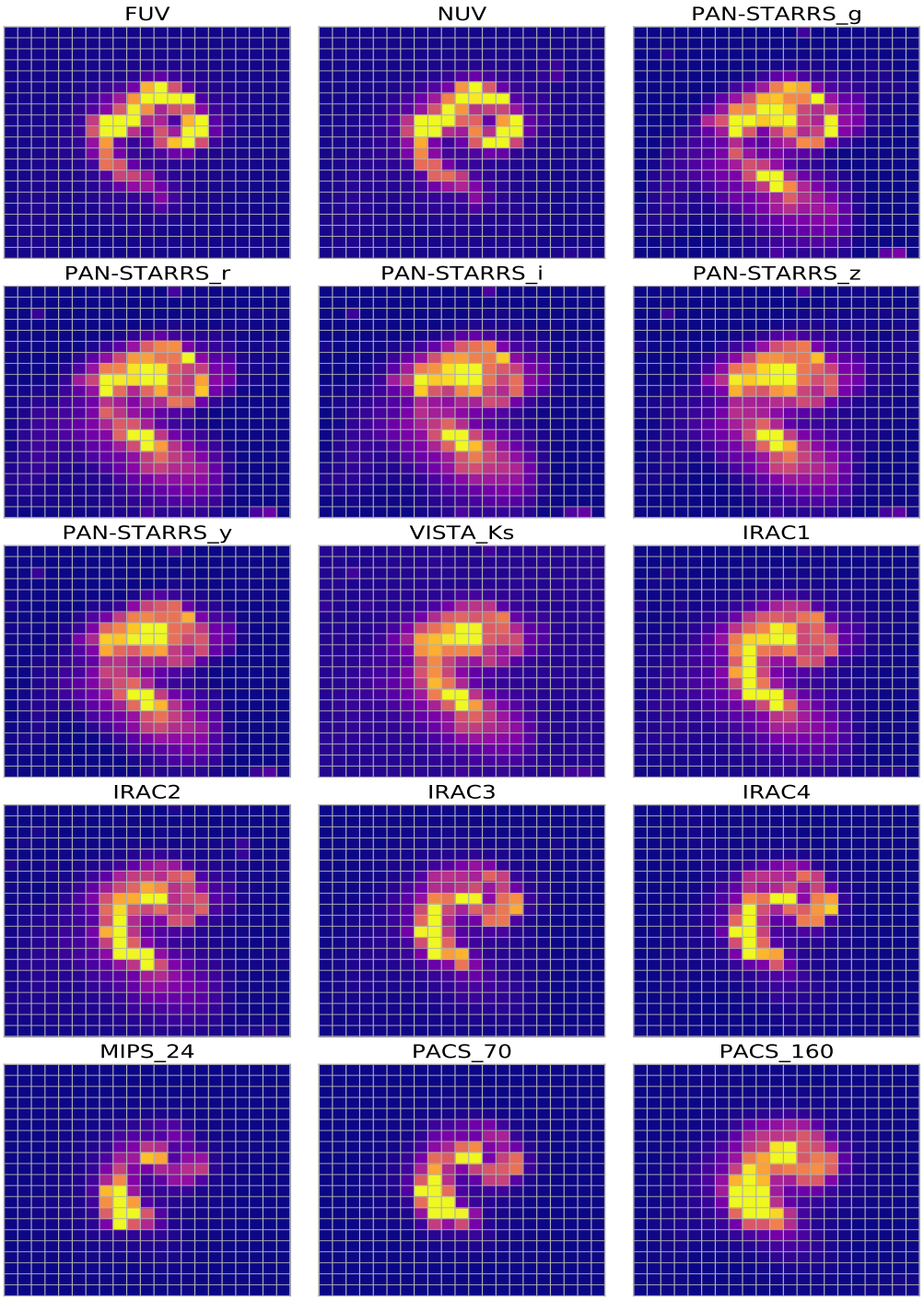

Fig. 1. Images of the Antennae Galaxies in the 15 different bands downgraded to the resolution of the 160 μm image.

3 Spectral energy distribution fitting

We analyse individual SEDs of the regions and the integrated SED corresponding to the sum of fluxes over the 58 regions. To fit the SEDs, we use the modelling software CIGALE (`https://cigale.lam.fr/version-2020.0/`). The code combines a stellar SED with dust attenuation and emission components and conserves the energy between the stellar dust absorption and dust re-emission to compute the final SED. We are mostly interested in studying the parameters linked to star formation and attenuation as the latter is critical in a dust-obscured objects such as the Antennae, so we focus our analysis on the following parameters: the stellar mass, the stellar mass of the bursting population, the SFR, the attenuation in the visible band and its slope.

SEDs can exhibit completely different features depending on the environment: there is much more intrinsic UV and far-IR emission for the region in the Overlap compared to the region in the nucleus of NGC 4038 (Fig. 2). Whitmore & Schweizer (1995) showed that the Overlap Region does hosts numerous star forming regions which lead to the observed level of intrinsic UV emission in this region. A large fraction of the UV light emitted is absorbed by dust as shown in the SED of region 47 and re-emitted in the infrared. In the region of the nucleus, this effect still occurs but on a smaller scale.

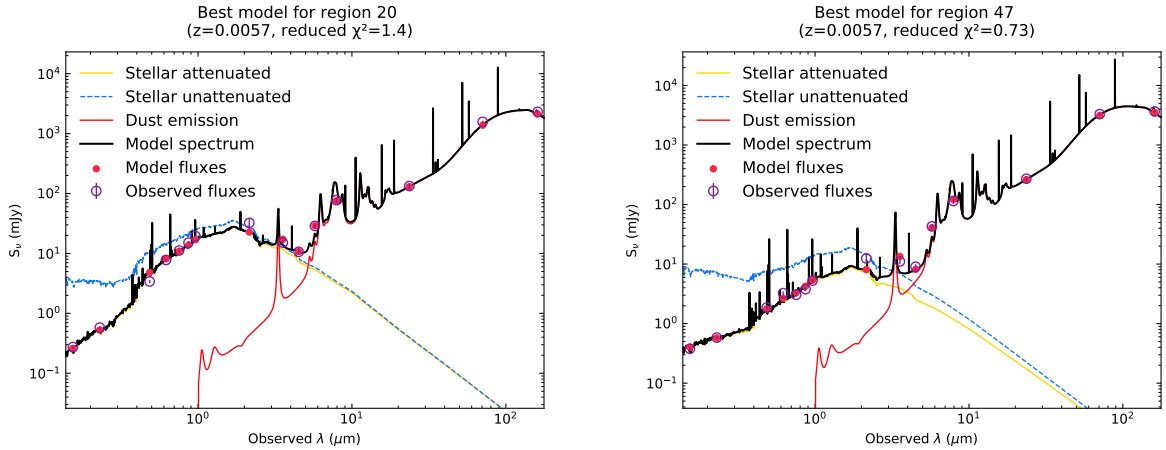

Fig. 2. Left: SED of a region of the nucleus of NGC 4038. **Right:** SED of a region part of the Overlap.

4 Physical parameters estimations

Below, we present the maps of the spatial distribution of the attenuation and the SFR in Fig. 3 and of the stellar mass and the mass of the bursting population in Fig. 4. We over-plotted coloured contours to separate the three components of the galaxies : blue for NGC 4038, red for NGC 4039 and green for the Overlap. The high levels of attenuation matches the high SFR in the Overlap and the beginning of the mass stripping from the nucleus of NGC 4039 can even be seen on the map of the stellar mass.

In Table 1, we compare the estimates of the parameters when the values obtained for the 58 regions are added to whose obtained when the whole system is fitted as a single source. We can see that the mean or summed values are in agreement with those derived for the whole system. This agreement is critical because each single derived parameter spans a wide range of values in the individual 58 regions due to the very perturbed nature of the Antennae. However, we find that Arp 244 as a whole does not exhibit values typical of high redshift galaxies. The Antennae Galaxies are a good proxy for high redshift perturbed objects but should not be confused as one.

5 Conclusions

We compare the estimates of the physical parameters obtained with the 58 regions added to those obtained for Arp 244 as a whole and we find a good agreement showing that the inability to resolve distant objects does not hinder CIGALE estimations. We are able to reliably estimate physical parameters like the star formation rate, the stellar mass and the dust attenuation even when in the case of the integrated SED. From our study of Arp 244, we conclude that the use of a SED fitting tool which preserves the energy balance between stellar and

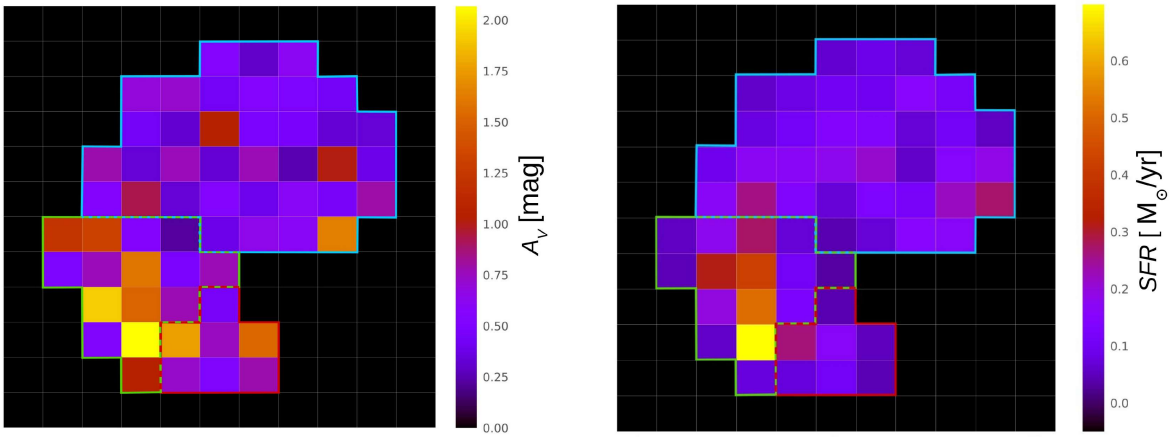

Fig. 3. Left: V-band attenuation. **Right:** Star formation rate.

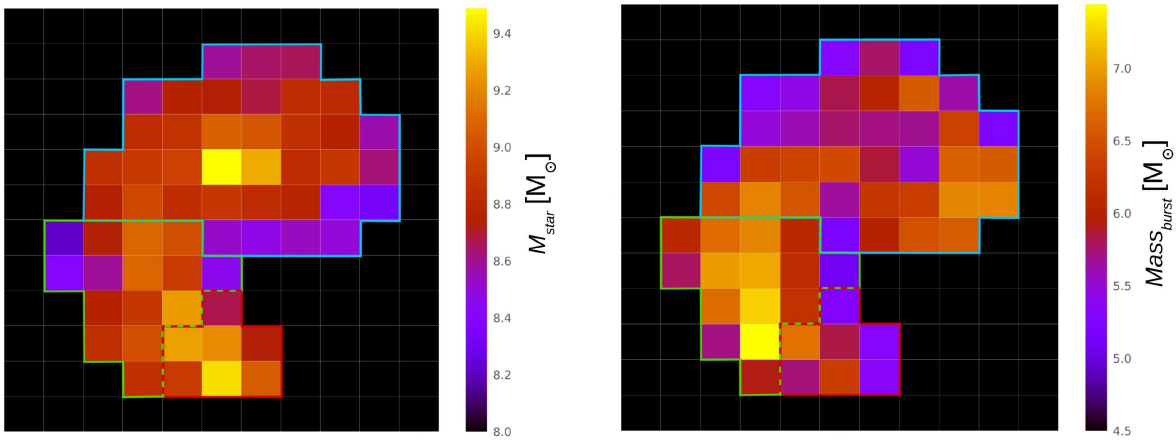

Fig. 4. Left: Logarithmic stellar mass. **Right:** Logarithmic mass of the bursting population.

Parameter	Mean (1σ)	58 fluxes added (1σ)	GS1 (z = 2.19) (1σ)
Mass of the bursting population (10^7 $M_\odot$)	17.04 ($\pm$ 4.50)	12.05 ($\pm$ 2.42)	38.92 ($\pm$ 25.75)
V-band attenuation	0.73 ($\pm$ 0.08)	0.68 ($\pm$ 0.10)	2.23 ($\pm$ 0.03)
Power law slope of dust attenuation in the ISM	-0.62 ($\mp$ 0.25)	-0.70 ($\mp$ 0.22)	-0.48 (fixed)
Star formation rate ($M_\odot$ yr^{-1})	8.50 ($\pm$ 1.01)	8.21 ($\pm$ 1.53)	218 ($\pm$ 14)
Stellar mass (10^9 $M_\odot$)	45.8 ($\pm$ 13.0)	40.5 ($\pm$ 9.5)	55.6 ($\pm$ 10.3)

Table 1. Values of the SFR, stellar mass and mass of the bursting population of the 58 regions in the second column are added to allow for a comparison with integrated values. Credit to V. Buat for the values of GS1.

dust emission such as CIGALE to measure global physical parameters gives robust results despite the highly inhomogeneous distributions of UV-optical and dust emission across the system.

References

Calzetti, D., Armus, L., Bohlin, R. C., et al. 2000, ApJ, 533, 682
Charlot, S. & Fall, S. M. 2000, ApJ, 539, 718
Elbaz, D., Leiton, R., Nagar, N., et al. 2018, A&A, 616, A110
Whitmore, B. C. & Schweizer, F. 1995, AJ, 109, 960